Journal of Neuroscience Methods 179 (2009) 208–218

Contents lists available at ScienceDirect

Journal of Neuroscience Methods

journal homepage: www.elsevier.com/locate/jneumeth

Intracranial microprobe for evaluating neuro-hemodynamic coupling in unanesthetized human neocortex

Corey J. Keller[a,c,*], Sydney S. Cash[a], Suresh Narayanan[a], Chunmao Wang[b], Ruben Kuzniecky[b], Chad Carlson[b], Orrin Devinsky[b], Thomas Thesen[b], Werner Doyle[b], Angelo Sassaroli[c], David A. Boas[d], Istvan Ulbert[e,f], Eric Halgren[g]

[a] Department of Neurology, Massachusetts General Hospital, Boston, MA, USA
[b] Comprehensive Epilepsy Center, New York University Langone Medical Center, New York, NY, USA
[c] Department of Biomedical Engineering, Tufts University, Medford, MA, USA
[d] Athinoula A. Martinos Center for Biomedical Imaging, Harvard Medical School, Charlestown, MA, USA
[e] Institute for Psychology of the Hungarian Academy of Sciences, Budapest, Hungary
[f] Peter Pazmany Catholic University, Department of Information Technology, Budapest, Hungary
[g] Multimodal Imaging Laboratory, Department of Radiology, University of California at San Diego, La Jolla, CA, USA

ARTICLE INFO

Article history:
Received 12 November 2008
Received in revised form 27 January 2009
Accepted 29 January 2009

Keywords:
Microelectrode
BOLD
Oxygenation
Hemodynamics
Neuro-hemodynamic coupling
Breath-hold
Electrocardiogram
Cortical electrical stimulation

ABSTRACT

Measurement of the blood-oxygen-level dependent (BOLD) response with fMRI has revolutionized cognitive neuroscience and is increasingly important in clinical care. The BOLD response reflects changes in deoxy-hemoglobin concentration, blood volume, and blood flow. These hemodynamic changes ultimately result from neuronal firing and synaptic activity, but the linkage between these domains is complex, poorly understood, and may differ across species, cortical areas, diseases, and cognitive states. We describe here a technique that can measure neural and hemodynamic changes simultaneously from cortical microdomains in waking humans. We utilize a "laminar optode," a linear array of microelectrodes for electrophysiological measures paired with a micro-optical device for hemodynamic measurements. Optical measurements include laser Doppler to estimate cerebral blood flow as well as point spectroscopy to estimate oxy- and deoxy-hemoglobin concentrations. The microelectrode array records local field potential gradients (PG) and multi-unit activity (MUA) at 24 locations spanning the cortical depth, permitting estimation of population trans-membrane current flows (Current Source Density, CSD) and population cell firing in each cortical lamina. Comparison of the laminar CSD/MUA profile with the origins and terminations of cortical circuits allows activity in specific neuronal circuits to be inferred and then directly compared to hemodynamics. Access is obtained in epileptic patients during diagnostic evaluation for surgical therapy. Validation tests with relatively well-understood manipulations (EKG, breath-holding, cortical electrical stimulation) demonstrate the expected responses. This device can provide a new and robust means for obtaining detailed, quantitative data for defining neurovascular coupling in awake humans.

1. Introduction

In recent years, studying brain activation with non-invasive functional MRI (fMRI) has become an essential tool in the field of neuroscience. However, the utility of fMRI is limited because it measures hemodynamic responses that have an unknown relationship to the electrophysiological activity that is used for neural information processing. We describe here a method for simultaneous quantitative measurement of both domains at the level of the cortical column in awake humans. These measurements may be used to calculate the transfer function between vascular and electrophysiological changes, and thus allow more precise interpretation of non-invasive hemodynamic results.

fMRI measures the blood-oxygenation-level dependent (BOLD) response. The neural basis of the BOLD signal is the focus of very active studies and has been reviewed previously (Logothesis and Wandell, 2004; Nair, 2005; Logothesis, 2007). The iron in hemoglobin (Hb) strongly affects the spin of nearby protons, but

* Corresponding author at: Department of Neurology, Massachusetts General Hospital, Boston, MA, USA. Tel.: +1 802 578 6292.
E-mail addresses: cjkeller@partners.org (C.J. Keller), scash@partners.org (S.S. Cash), suresh.narayanan@ge.com (S. Narayanan), wangch@nidcd.nih.gov (C. Wang), ruben.kuzniecky@med.nyu.edu (R. Kuzniecky), ccarlso2@gmail.com (C. Carlson), od4@nyu.edu (O. Devinsky), thomas.thesen@med.nyu.edu (T. Thesen), wkd1@nyu.edu (W. Doyle), angelo.sassaroli@tufts.edu (A. Sassaroli), dboas@nmr.mgh.harvard.edu (D.A. Boas), ulbert@cogpsyphy.hu (I. Ulbert), ehalgren@ucsd.edu (E. Halgren).

0165-0270/$ – see front matter © 2009 Elsevier B.V. All rights reserved.
doi:10.1016/j.jneumeth.2009.01.036

not if it is shielded by oxygen, i.e., in oxy-hemoglobin (Hbo). Thus, the BOLD signal ultimately reflects changes in concentration of paramagnetic deoxy-hemoglobin (Hbr) (Ogawa et al., 1990). The concentration of Hbr, Hbo, and total Hb (Hbt) depends on the local cerebral metabolic rate for oxygen ($LCMRO_2$), cerebral blood volume (CBV), and the rate of regional cerebral blood flow (rCBF). Thus, the BOLD signal can be precisely modeled from these measures (Buxton et al., 1998). Since changes in rCBF and CBV are thought to be coupled (Grubb et al., 1974), and $LCMRO_2$'s effects are reflected in blood oxygenation (Hoge et al., 1999; Mandeville et al., 1999; Waldvogel et al., 2000; Jones et al., 2001), the critical hemodynamic measures are rCBF, Hbr, and Hbo.

It is known that neural activity triggers an increase in $LCMRO_2$. Shortly thereafter, an increase in rCBF is observed that overcompensates for the increased $LCMRO_2$ and as a result Hbr eventually decreases. Although the exact aspect of neural activity that triggers and controls these hemodynamic changes has been extensively studied, the underlying mechanisms involved are still under debate (Hewson-Stoate et al., 2004; Dunn et al., 2005; Logothesis, 2003; Buzsaki et al., 2007). Some studies describe a linear neurovascular coupling (Martindale et al., 2003; Sheth et al., 2003), while others report a non-linear relationship when stimulation parameters are varied over a wider range (Devor et al., 2003; Jones et al., 2004). It has also been reported that the BOLD signal correlates with spiking activity (Rees et al., 2000; Heeger et al., 2000), although the preponderance of evidence supports a correlation with synaptic activity (Logothesis et al., 2001; Galuske et al., 2005; Mukamel et al., 2005). Equally controversial, groups have found that a stimulus-evoked negative BOLD response is a result of neuronal inhibition (Schmuel et al., 2006; Devor et al., 2007), while others support a vascular steal interpretation (Harel et al., 2002). Additionally, the "initial dip" continues to be highly controversial, primarily because this decrease in Hbo and increase in Hbr prior to any change in CBF has been reproducible in several studies (Vanzetta and Grinvald, 1999; Mayhew et al., 2000; Jones et al., 2001) while others have found no evidence of its presence (Lindauer et al., 2001). In order to further understand the "initial dip" which will strengthen fMRI studies on human brain function, the basic physiology of neurovascular coupling must be addressed (Buxton, 2001).

Based on the complexity of these relationships, with critical parameters that may vary between species and components of cognitive activation that differ in anatomical location, latency, and behavioral correlates, it is essential that the inter-relations of neuronal activity and hemodynamics be measured directly in humans during cognition.

Hemodynamic responses to neuronal activation appear to be controlled at the level of a vascular unit, where rCBF is regulated by changing the contraction of smooth muscles in arteriole walls. Anatomically, a vascular unit supplies one or a few cortical columns. While individual measurement of all $\sim 10^5$ neurons and $\sim 10^9$ synapses within this volume is clearly beyond current technology, effective population measures based on microelectrode arrays have been developed. The different populations of cortical neurons, as well as their inputs from different areas, tend to be segregated into layers (Felleman and VanEssen, 1991). Firing by these different populations can be estimated with microelectrode arrays sampling multi-unit activity (MUA) in different cortical layers, and trans-membrane neuronal current flows associated with activation of these different synaptic inputs can be estimated from the second spatial derivative of the field potentials recorded by the same contacts (Current Source Density, CSD, Nicholson and Freeman, 1975; Ulbert et al., 2001a,b; Einevoll et al., 2007). Quantification of trans-membrane current is of particular interest since restoring ionic balance is the largest single process consuming energy in the brain (Attwell and Iadecola, 2002). In addition, MUA measurement allows interpretation of CSD currents as excitatory or inhibitory.

Cortical point spectroscopy allows recording of local hemoglobin concentration changes by utilizing absorption and scattering properties of Hbo and Hbr in tissues (Dunn et al., 2005). While hemodynamic concentration changes are a critical component of the BOLD response, blood flow is also involved and is not monitored by spectroscopy. Therefore, simultaneous blood flow measurements will be acquired using the laser Doppler flowmetry (LDF) technique, which permits regional cerebral blood flow measurements from changes in the flux of red blood cells in microvasculature (Bonner and Nossal, 1981). Measuring simultaneous local blood flow and oxygenation will provide a further understanding of the complex relationship between hemodynamics, metabolic activity, and the BOLD response.

It is with this motivation that we present a novel device that allows for robust semi-chronic intracranial recordings of the human neocortex that incorporates simultaneous neuronal and optical measurements at the level of the cortical microcolumn. A multicontact microelectrode array inserted perpendicularly to the neocortex records PG and MUA while an optical emitter/detector pair senses blood flow and oxygenation. Design of this device is described and preliminary results are presented from *in vivo* responses of EKG, breath-holding, and cortical stimulation.

2. Materials and methods

2.1. Microelectrode design

Construction and use of the laminar microelectrode have been described previously (Ulbert et al., 2001a,b). Briefly, 24 platinum iridium (90/10%) contacts 40 μm in diameter are equally spaced at 150 μm centers to span the 3.6 mm width of the gyral grey matter (Fig. 1a, b). The microelectrode array is embedded in a polyimide-epoxy substrate with total outer diameter of 350 μm. A thin square made of silicone with surface area of $\sim 1\,cm^2$ is attached at the top of the microelectrode, and surface tension between the surface square and the cortical surface assists in securing the microprobe in position. Output leads are embedded in silicone and attached to a 26-pole ribbon cable connector. Intercontact impedance is $1\,M\Omega \pm 10\%$ at 100 Hz and thermal noise is 7.5 μV in EEG range and 20 μV in MUA range.

2.2. Optical microprobe design

The optical component of the device consists of an emitter and detector fiber optic unit embedded in the silicone sheet and is able to probe activity in the microcolumns surrounding the microelectrode. Both fiber bundles (F2 core/8250 cladding, 50 μm diameter, 300 fibers, 1 mm total diameter, Fiberoptix Technology, Pomfret, CT) run parallel to the cortical surface. Fiber bundle diameter was chosen to be 1 mm, small enough to not hinder clinical recordings when placed directly below the subdural electrode grid but able to carry significant light power. In order to re-direct light so the emitter and detector are parallel to the cortical surface, dichroic prisms (PN #716603, Westchester Technologies, Peekskill, NY) were assembled at the termination of the fibers. The prisms are cut at a 45° angle and silvered in order to direct the light downward from the emitter or upward to the detector (Fig. 1a,b). Dichroic prisms lay above the cortex while the microelectrode array penetrates the pia and is oriented normal to the cortical surface. In order to develop a probe with the safety and resolution necessary to meet the above requirements, each component of the microprobe including wavelength range, optical fiber size, and emitter-detector separation distance was considered.

When spectroscopy is used for Hbr and Hbt measurements from the scalp, the main design limitation is photon penetration, and thus infrared wavelengths from 650 to 900 nm are used. However,

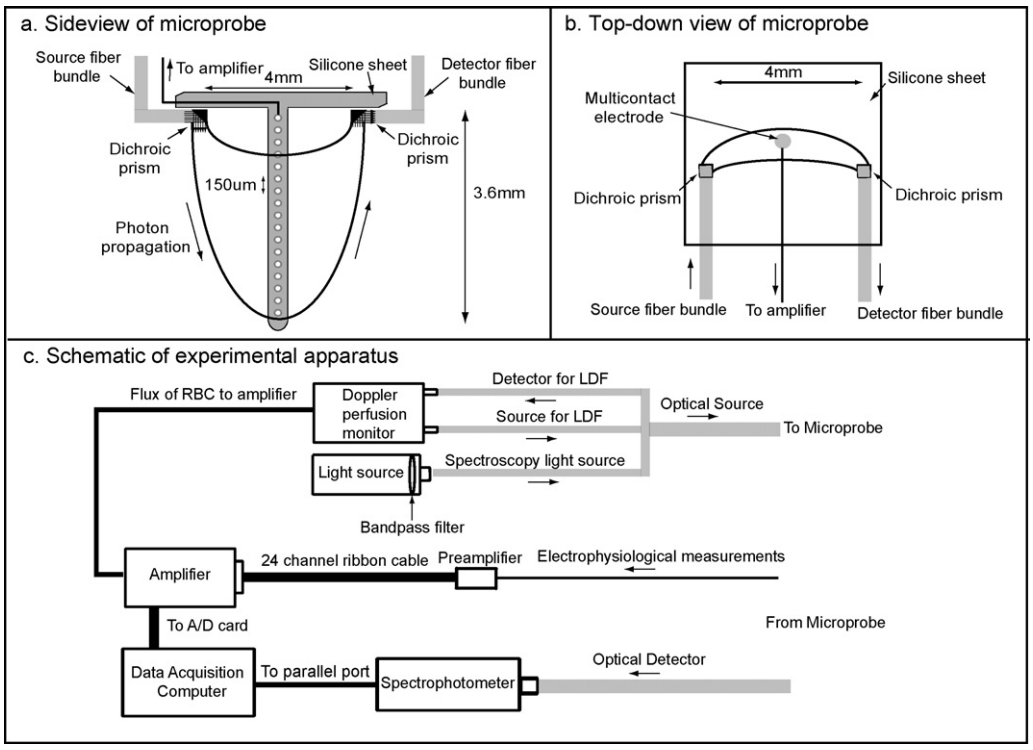

Fig. 1. Schematic of the laminar optode and experimental apparatus. (a, b) Side and top-down views of device. The laminar optode consists of a 3.6 mm long 24-contact shaft that spans the cortical grey matter at the gyral crown. In addition, an emitter-detector pair probes the tissue surrounding the shaft. The path of light can be modeled by a banana-shaped curve. (c) Schematic of experimental apparatus. Grey lines indicate fiber bundles. Light for Doppler and spectroscopy measurements mix and are transmitted to the cortex. Scattered light for both modalities as well as amplified and filtered electrophysiological measurements are simultaneously transmitted to the acquisition computer.

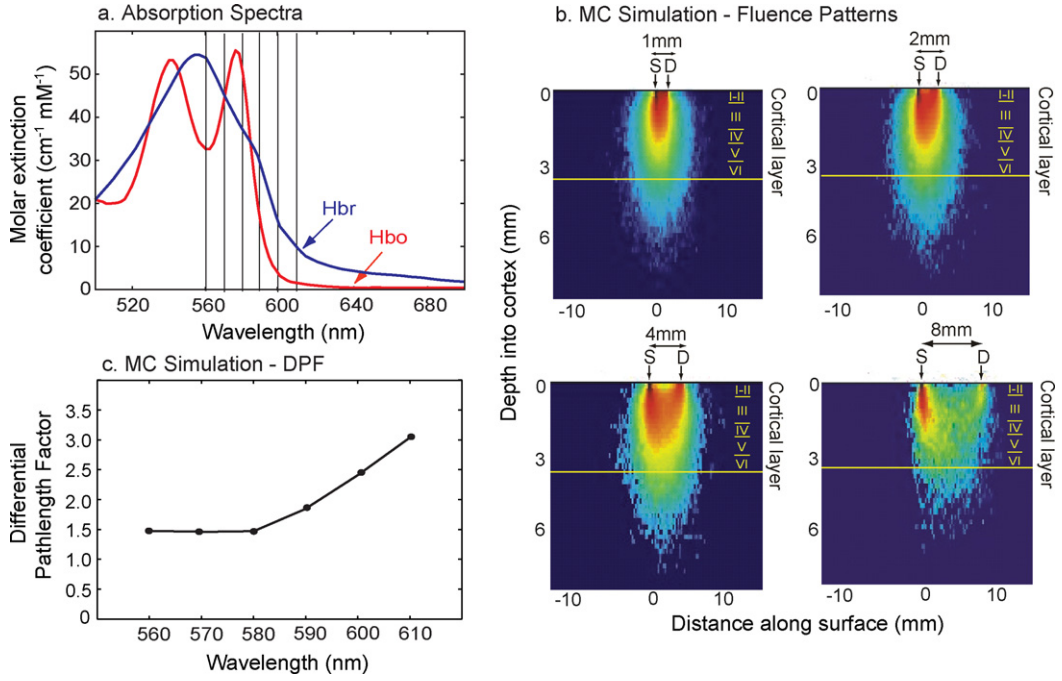

Fig. 2. Calculation of absorption spectra, photon propagation, and the differential path length factor. These model calculations were used to guide the choices of wavelength range, sensor separations, and spectroscopic calculations. (a) Absorption coefficients for oxy- and deoxy-hemoglobin for the visible light range offers higher absorption and greater variability to calculate hemodynamic concentrations compared to the near-infrared region above 700 nm. Vertical lines denote bandpass filters used for spectroscopy calculations. (b) Simulated normalized fluence patterns for 1, 2, 4 and 8 mm separations. At a separation distance of 4 mm, measurement of light absorption is sufficient to sample the entire depth of the cortex without undue lateral spread. (c) The differential path length factor for wavelengths in the visible light range accounts for absorption and scattering changes due to wavelength property differences.

optical probes directly implanted in the target organ are not limited by the distance of wavelength penetration (Obrig et al., 2003). Wavelengths in the visible light range, specifically 560 to 610 nm, offer an increased sensitivity to hemodynamic changes compared to the near-infrared range due to high absorption coefficients in this region (Fig. 2a). In addition, less than 10% of scattering is due to chromophores other than hemoglobin and water. This spectral range also has the advantage of including wavelengths highly selective for Hbt and Hbr. Specifically, within this range, isobestic points (525, 545, 570, and 583 nm) are sensitive to Hbt changes while 610 nm is sensitive to Hbr changes (Haglund and Hochman, 2004).

In order to determine the emitter-detector separation distance that will sample the six layers of the neocortex without undue lateral spread, the algorithm established by Kohl et al. (2000) was applied to conduct Monte Carlo simulations and determine the fluence patterns in this spectral range. Monte Carlo simulations calculate the direction and path length of each photon reaching the detector within its acceptance angle and the fluence through each voxel in the semi-infinite geometry used. For the simulation, a single emitter was placed on the pial surface with four detectors in a linear array 1, 2, 4, and 8 mm from the emitter. The cortex was modeled as a semi-infinite homogeneous tissue with uniform scattering coefficient $\mu_s = 10\,\text{mm}^{-1}$, absorption coefficient $\mu_a = 0.1\,\text{mm}^{-1}$, and an anisotropic factor of $g = 0.9$. Twenty-five million photons were used for this simulation. The fluence of the detected photons was calculated as

$$\phi(t) = \frac{1}{N_{\text{photons}}(t)} \sum_{i=1}^{N_{\text{photons}}(t)} \prod_{j=1}^{N_{\text{regions}}} e^{(-\mu_{a,i} L_{i,j})} \quad (1)$$

where $\Phi(t)$ is the measured photon fluence at detector j, N_{photons} is the number of photons injected into the medium, $e^{(-\mu a,iLi,j)}$ corrects for the effects of absorption in each region where $L_{i,j}$ is the path length of photon i through region j, and N_{regions} is the number of regions through which the photons migrate (Boas et al., 2002; Custo et al., 2006). The depth profile of sampling, as indicated by the normalized fluence patterns (Fig. 2b), increases from one to two to four mm separation before deteriorating somewhat at 8 mm. These Monte Carlo simulations revealed that the measurements of light absorption sufficient to sample the entire depth of the cortex without undue lateral spread and relatively uniform layer sampling are possible with an emitter-detector separation of 4 mm.

The mean penetration depth $\langle z \rangle$ of photons can also be calculated for various emitter-detector separations and is defined as

$$\langle z \rangle = \frac{\sqrt{d/\mu_{\text{eff}}}}{2} \text{ where } \mu_{\text{eff}} = \sqrt{3\mu_a \mu_s'} \text{ and } \mu_s' = \mu_s(1-g) \quad (2)$$

where d is the emitter-detector separation, μ_{eff} is the effective attenuation coefficient, μ_s' is the reduced scattering coefficient calculated to be $1\,\text{mm}^{-1}$, and g is the anisotropy factor (Patterson et al., 1995). The mean penetration depth for 1, 2, 4, and 8 mm emitter-detector separations were calculated to be 1.2 1.7, 2.4, and 3.4 mm, respectively. At a mean penetration depth of 2.4 mm with a 4 mm emitter-detector separation, the majority of photons will transverse layer IV–V where pyramidal cell bodies reside. In addition, cortical layers above and below are also sufficiently sampled. Therefore, based on the fluence patterns and mean penetration depth calculations, a 4 mm separation distance was chosen for this device.

2.3. Data acquisition system and analysis

An overview of the recording apparatus and analysis approach will be described here, followed by specific details in later sections concerned with different measurement modalities and validation tests. The schematic diagram of the experimental setup is shown in Fig. 1c. Briefly, two light sources used for blood flow and hemodynamic measurements are mixed and sent into the cortex. Reflected light is analyzed with a photomultiplier for hemodynamic changes and a perfusion monitor for blood flow recordings. Simultaneous electrophysiological information is transmitted from the microelectrode into the amplifier where it is isolated and filtered into low (PG, 0.5–500 Hz) and high (MUA, 500 Hz–20 kHz) frequency signals. All information is transmitted to the data acquisition computer using a custom-written Labview program (National Instruments, Inc.). Additionally, isolation boxes allow safe synchronization of the microprobe measurements with clinical recordings.

Data management and a stepwise approach are necessary when recording simultaneously with multiple modalities. The dynamics of population neuronal input and output in different cortical layers are first estimated from current source density and multiunit activity, respectively. Simultaneous hemodynamic parameters including rCBF, Hbo, Hbr, and Hbt in the same tissue are then calculated from the optical measures. Finally, electrophysiological and hemodynamic parameters are related.

2.4. Estimation of population trans-membrane current flows in different cortical layers

Population synaptic activity as well as slow voltage-gated active channels directly produce trans-membrane current flows (Murakami et al., 2002) which were estimated using current source density (CSD) analysis (Freeman and Nicholson, 1975). Assuming that the currents are radially symmetric around the laminar electrode trajectory, CSD is calculated as the second spatial derivative of field potentials (0.5–30 Hz) after applying a 5-point Hamming filter (Ulbert et al., 2001a,b). CSD analysis assumes that conductivity is uniform and isotropic in the tissue immediately surrounding the probe (Mitzdorf, 1985). This assumption has been tested in the hippocampus where deviations from the homogeneous approximation were found to be too small to influence the spatial distribution of sources and sinks (Holsheimer, 1987). Variable electrode spacing or potential amplification could produce spurious CSD signals but these effects were evaluated experimentally in our system and found to be less than 5% (Ulbert et al., 2001a,b). CSD analysis will miss trans-membrane currents if they do result in a net radial extracellular current, as might happen if they are produced by synapses on a spherically symmetrical dendritic domain. CSD will also fail to detect currents that flow over distances that are small relative to the spatial sampling density. Modeling and experimental measures indicate that the center-to-center contact spacing of 150 μm used in the current study is adequate to sample laminar CSD in macaque primary visual cortex (Schroeder et al., 1998; Tenke et al., 2003). The limiting factor was the dendritic domains of stellate cells in thalamorecipient layer IVc. Cortex is thicker in humans, and the sampled areas are not known to have a thin but important sublayer comparable to IVc. Nonetheless, it is likely that the CSD analysis reported here is relatively insensitive to synaptic activity on layer IV stellate cells. Explicit models accounting for the effects of the differences in conductivity above and below the cortical grey matter, as well as the limited radial extent of the sink, have been described (Peterson et al., 2006; Einevoll et al., 2007). Finally, current sources or sinks can be missed if the laminar probe does not sample the entire cortical depth.

2.5. Laser Doppler flowmetry

LDF was carried out using the MoorLab Server (MoorLAB Server, Devon, UK). LDF has excellent temporal resolution and allows continuous recording of red blood cell changes in microvasculature. It is based on the principle that low power coherent light (780 nm) is scattered by moving red blood cells and the backscattered light is frequency broadened (Bonner and Nossal, 1981). This light coupled

with scattered light from tissue is high pass filtered (700 nm cutoff) and subsequently collected by a photodetector at 40 Hz, digitized, and processed to produce a measure of the flux of red blood cells, correlated with rCBF.

2.6. Cortical point spectroscopy

Light from a halogen light source (HL-2000, Tungsten Halogen Light Source, Ocean Optics, Dunedin, FL) is sent into the cortex and reflected light is gathered and sent to a photomultiplier (S2000, Ocean Optics, Dunedin, Florida) where it is split into 360 frequency bands 0.5 nm wide. Counts are integrated at adjustable frame rates from 10 to 20 Hz. The recording frequency was set based on the signal-to-noise ratio of the recording and was determined to be acceptable at 1000 counts. At this frequency range the cardiac pulse and low frequency hemodyamic responses can be monitored, and the onset of response to stimulation can be sufficiently measured.

The Modified Beer Lambert Law relates the changes in reflection spectra of the tissue with concentration changes in the chromophores in the tissue:

$$\Delta A(\lambda) = \log_{10}\left(\frac{R_0}{R}\right) = \sum_i (\varepsilon_i(\lambda)\,\Delta c_i)\mathrm{DPF}(\lambda) \tag{3}$$

where $\Delta A(\lambda)$ is the attenuation at a given wavelength, ε_i is extinction coefficient of the ith chromophore, Δc_i is the change in concentration of the ith chromophore, DPF is the differential pathlength factor, and R_0 and R are the initial reflectance and reflectance at time t, respectively, for a given wavelength λ. Extinction coefficients used for Hbr and Hbo were previously established (Wray et al., 1988).

A Monte Carlo simulation was conducted to determine the DPF (Sassaroli et al., 2006), necessary to accurately calculate chromophore concentration changes in (3). The DPF accounts for the different optical path lengths through the tissue due to the different absorption and scattering at varying wavelengths. MIE theory calculates the angular probability distribution (phase function) of the single scattering event due to a spherical particle suspended in a homogeneous medium. Baseline scattering properties were $\mu_s = 10\,\mathrm{mm}^{-1}$ and $g = 0.9$, and the emitter-detector separation of 4 mm determined from the fluence maps (Fig. 2b) were used. The Monte Carlo simulation output of the DPF as a function of wavelength can be found in Fig. 2c.

Estimation of hemodynamic variables from spectroscopic measurements using wavelengths in the range of 500–650 nm is not as established as when using the near-infrared range where 690 and 830 nm are frequently chosen. Reasons for recording in the visible spectra are described earlier. In order to minimize possible errors in our hemodynamic calculations, a least squares approach was implemented as described previously (Dunn et al., 2005). Six wavelengths with 10 nm separations from 560 to 610 nm were used for this linear regression (Fig. 2a). By measuring the reflectance spectra (R_0/R) from these wavelengths, we can identify the change in Hbr and Hbo over time. This can be written in a matrix format as

$$y(\lambda,t) = \begin{bmatrix} \Delta A(\lambda_1) \\ \Delta A(\lambda_2) \\ \cdot \\ \cdot \end{bmatrix} = \begin{bmatrix} \varepsilon_{\mathrm{Hb}}^{\lambda_1} & \varepsilon_{\mathrm{HbO}}^{\lambda_1} \\ \varepsilon_{\mathrm{Hb}}^{\lambda_2} & \varepsilon_{\mathrm{HbO}}^{\lambda_2} \\ \cdot & \cdot \\ \cdot & \cdot \end{bmatrix} \begin{bmatrix} \Delta c_{\mathrm{Hb}}^{t_1} & \Delta c_{\mathrm{Hb}}^{t_2} & \cdots \\ \Delta c_{\mathrm{HbO}}^{t_1} & \Delta c_{\mathrm{HbO}}^{t_2} & \cdots \end{bmatrix} = F(\lambda)x(t) \tag{4}$$

The Hbr and Hbo time course can be computed from the equation as a minimum norm solution given by

$$\begin{bmatrix} \Delta c_{\mathrm{Hb}}^{t_1} & \Delta c_{\mathrm{Hb}}^{t_2} & \cdots \\ \Delta c_{\mathrm{HbO}}^{t_1} & \Delta c_{\mathrm{HbO}}^{t_2} & \cdots \end{bmatrix} = x(t) = (F^t F)^{-1} F^T y(\lambda,t) \tag{5}$$

This algorithm permits accurate hemodynamic estimates to be calculated from measurements in less commonly utilized spectral ranges.

2.7. Breath-hold experimental paradigm

Prior to the breath-hold challenge, patients were informed of the details of the experiment and asked to avoid head movement during the task. At the beginning of each of three 150 s cycles patients were asked to breathe normally until visual and auditory cues prompted a 30 s breath-hold. Each cycle was separated by 120 s of normal breathing to allow physiological parameters to return to baseline. Hemodynamic measurements were acquired via the data acquisition system. End-tidal CO_2 (PET_{CO_2}) was sampled from a leak-free mask and analyzed (CardioPulmonary Technologies, Sussex, WI) to validate the breath-hold.

2.8. Electrical stimulation

The subdural grid electrodes are commonly stimulated with low level electrical currents as part of the clinical protocol in order to reproduce elements of the clinical manifestations of the seizure, or to map regions of eloquent cortex (Ojemann, 1991). Individual clinical grid contacts (4 mm diameter disk, Adtech Medical Inc.) were stimulated with varying duration and amplitude well below the safety threshold: stimuli were isolated, charge balanced, biphasic, and constant current, with a charge density per phase below 50 $\mu C/cm^2$ (Lesser et al., 1987). Simultaneous electrical activity, blood flow, and oxygenation were measured with the microprobe during stimulation.

2.9. Surgical procedure

Patients with intractable epilepsy returning after a Phase 1 scalp EEG monitoring session undergo a craniotomy under general anesthesia followed by subdural grid electrode placement. The cortical area to be sampled was based on prior scalp EEG initial monitoring, ictal behavior, and other non-invasive tests (MRI, SPECT, PET). The laminar optode is first cleaned by dipping into EtOH for 30 s followed by 0.9% NaCl for 60 s and activated by applying +6 V against an Ag/AgCl electrode for 30 s in saline, thereby removing debris from electrode sites. It is then is cleaned in saline for 10 min to achieve stabilization of the double layer after which it is sterilized prior to implantation in a high temperature gas chamber (minimum 5 h, 130–180 °F) with a post sterilization settling time of 6 h (Ulbert et al., 2001a,b). During implantation, it is inserted normal to the cortical surface directly beneath the subdural grid, allowing surface tension to secure the microprobe in place. The location of the insertion is determined by the clinical team without regard for the research agenda and is targeted to a section of cortex which is expected to be resected at the time the patient returns to the OR for removal of epileptogenic cortex. The two optical fiber bundles and the output lead of the microelectrode are secured by stitching the leads to the edge of the bone. Although the fibers used were reasonably robust and able to handle the rigors of the clinical environment, great care is taken to minimize attenuation by not bending the fibers when securing in place. Post-operatively, glass fibers at the extracranial termination of fiber bundles are exposed, two component medical grade epoxy is applied (Epotek, Billerica, MA), and custom connectors

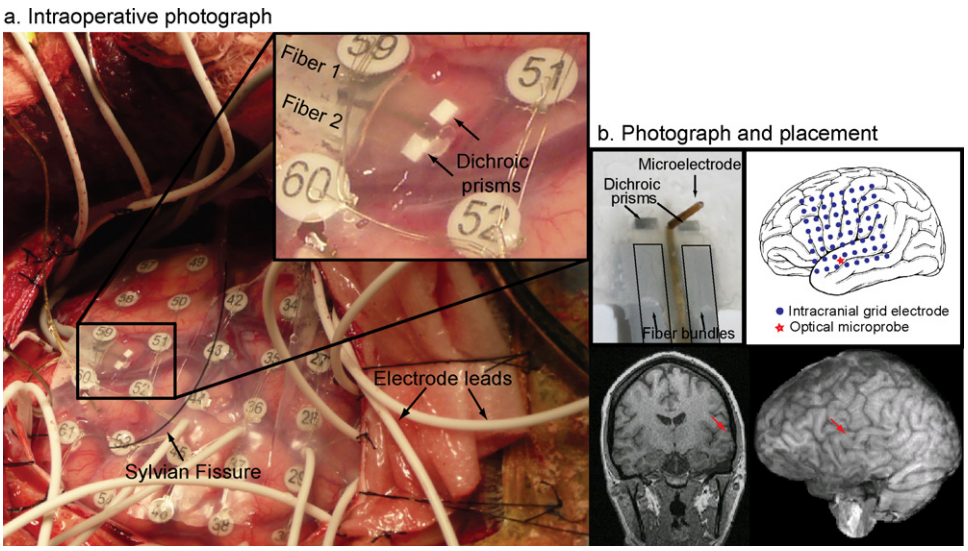

Fig. 3. (a) Intraoperative photograph of clinical grid electrodes and laminar optode. Subdural electrode arrays were placed to confirm the hypothesized seizure focus and locate epileptogenic tissue in relation to essential cortex, thus directing surgical treatment. The laminar optode device consists of a multicontact microelectrode coupled with emitter and detector fiber optic bundles that terminate at dichroic prisms. The microelectrode is inserted perpendicularly to the cortical surface to span the cortical grey matter layers. The dichroic mirrors at the termination of the fiber optic bundles lay beneath the grid electrodes on top of the pia. This microprobe was inserted into the left superior temporal gyrus in a patient with frontotemporal epilepsy. (b) From top-left clockwise: Photomicrograph of device, subdural grid electrodes and microprobe placement on standard brain, location on coronal view of MRI, location on 3D rendering of MRI.

attach the microprobe to the light guide assay. Semi-chronic spontaneous recordings span the duration of hospital admittance which ranges from 5 to 10 days. At the time of resection, cortical tissue surrounding the electrode can be removed *en bloc* and sent to pathology for staining with luxol fast blue, Bielschowsky, and hematoxilin and eosin in order to identify cortical laminae using standard criteria.

2.10. Patients and potential risks

Four patients (two females, ages 24–36) with long-standing pharmaco-resistant complex partial seizures participated after fully informed consent according to NIH guidelines as monitored by the local Institutional Review Board. Simultaneous scalp, macroelectrode, and microelectrode cortical recordings were made over the course of clinical monitoring for spontaneous seizures. Patients were all right handed with intelligence and personality in the normal range. The decision to implant, the electrode targets, and the duration of implantation were made entirely on clinical grounds without reference to this experiment. The patients were informed that participation in the experiment would not alter their clinical treatment in any way, and that they may withdraw at any time without jeopardizing their clinical care.

Minor risks associated with the microprobe implantation include intracranial hemorrhaging of a blood vessel and gliosis. Neurosurgeons trained in microelectrode placement techniques avoid placement in close proximity to blood vessels. In addition, strict adherence to sterilization protocol minimizes risk of infection. In any case, the microarray is placed in tissue that the patient's epileptologist anticipates will be removed in the definitive surgery.

Measures were taken to ensure that human tissue exposure to light is well within safety standards to avoid tissue damage. The fluence due to all wavelengths in the spectral range 500–650 nm was calculated to be 0.058 W/cm^2. Coupled with the peak power density due to laser Doppler measurements, 0.002 W/cm^2, the total optical fluence at the cortex is 0.060 W/cm^2, well below the maximum permissible exposure of 0.2 W/cm^2 for each wavelength in this range from a continuous wave laser for times larger than 10 s (see ANSI Standard Z136.1-1993).

3. Results

To date, this device has been successfully implanted in four patients with intractable epilepsy who are undergoing placement of subdural grid electrodes for clinical purposes. When implanted, the microprobe is positioned directly beneath the subdural grid and surface tension secures the optical fiber bundles and microprobe in place (Fig. 3a). EEG recordings from clinical contacts surrounding the microprobe were not compromised by the introduction of the device. The hemodynamic responses synchronized with both the electrocardiogram and a breath-holding task will be described as means to validate the technique. In addition, neural activity and hemodynamic changes recorded during cortical stimulation will be discussed.

3.1. Electrocardiogram and cerebral blood flow

The pulsatile cerebrovascular response, synchronized to the EKG, is a strong and reliable signal that has been used to validate various novel non-invasive and invasive hemodynamic measurement techniques (Montgomery et al., 1995; Basano et al., 2001; Zhang and Levine, 2006; Kucewicz et al., 2007). In each of these studies, an increase in rCBF was observed after each cardiac pulse, with a latency of 100–200 ms measured from the *R*-peak of the QRS wave to the initial increase in rCBF. Across these studies, the percent change in blood flow is often not consistent and in some cases not reported.

In order to determine the validity of the LDF measurements *in vivo*, simultaneous EKG and rCBF were monitored. Representative data from a continuous recording with the laminar optode can be found in Fig. 4a. An increase in rCBF ranging from 8 to 20% can be observed after each ventricular depolarization. An average (Fig. 4b) of 500 EKG pulses elucidates a 12% peak increase in blood flow, as well as a latency of 150 ms between the *R*-peak and rCBF increase,

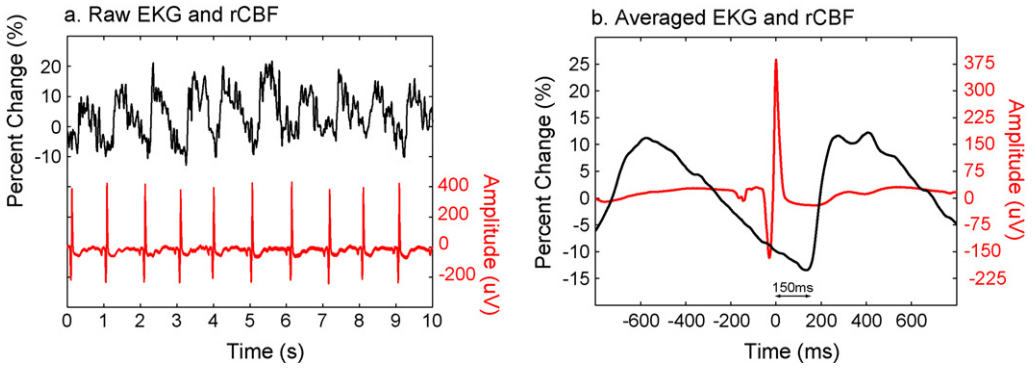

Fig. 4. (a) Representative data of continuous recording of electrocardiogram (EKG) and regional cerebral blood flow (rCBF) using laser Doppler flowmetry (LDF) with the laminar optode. Percent signal change of rCBF is on the left axis and EKG amplitude on the right. An 8–20% increase in rCBF is evident following ventricular depolarization. (b) EKG with percent change of rCBF averaged over 500 cardiac pulses demonstrates a 12% increase in rCBF peaking 150 ms after the *R*-peak in the QRS wave.

consistent with previous studies (Montgomery et al., 1995; Basano et al., 2001).

3.2. Breath-holding

Breath-holding is a simple cerebrovascular challenge commonly employed to validate fMRI and spectroscopy studies (Kastrup et al., 1999). Breath-holding induces a hypercapnic state, i.e., an elevated partial pressure of arterial carbon dioxide. Carbon dioxide acts as a vasodilator, producing a global increase in cerebral blood flow (Xie et al., 2005). During a breath-hold task, increases are commonly observed in the BOLD signal (Wise et al., 2007; Thomason et al., 2005), the FAIR signal (Flow-sensitive Alternating Inversion Recovery) relating rCBF values (Kastrup et al., 1999; MacIntosh et al., 2003), and Hbr and Hbt with near-infrared spectroscopy (NIRS, Safonova et al., 2003; MacIntosh et al., 2003).

One patient performed a breath-holding task consisting of three cycles of alternating normocapnic and hypercapnic events. Hemodynamic concentrations from the microprobe were recorded during the breath-hold challenge with simultaneous end-tidal CO_2 measurements (PET_{CO_2}) to corroborate results. Each cycle consisted of a 30 s breath-hold followed by 120 s of normal breathing, providing sufficient time for physiological components to return to baseline. Average hemodynamic concentration changes and PET_{CO_2} changes are shown in Fig. 5. Transparent colored curves indicate one standard deviation above and below average values. Dotted lines represent the start and end of the breath-hold while the grey area after the dotted lines indicates the latency before physiological change. As expected, increases in Hbr and Hbt and a decrease in Hbo were observed beginning approximately 5 s after breath-hold onset. These changes progressively increased until peaking 5 s after breath-hold termination and eventually settling back to normal physiological baseline values after a slight hyperoxygenation period. PET_{CO_2} values remained at 0% for the duration of the breath-hold and increased following the event, confirming that it was sufficient to elevate vascular CO_2 levels. The direction, timing, size, and coupling of these measures are consistent with the well-known neurovascular changes during hypercapnia and are discussed later.

3.3. Cortical electrical stimulation

Direct cortical electrical stimulation is commonly employed in patients with intractable epilepsy undergoing surgery in order to localize functional brain areas (Ojemann, 1991). If cortical stimulation results in a behavioral deficit then the stimulated cortex is inferred to contribute to the tested behavior (Halgren et al., 1985). Cortical stimulation may also produce sensory or motor activity by stimulation of sensory or motor cortices, or complex mental phenomena by stimulation of limbic cortex (Halgren et al., 1978a,b). The clinician will vary stimulation amplitude, duration, and inter-stimulus interval in order to probe the functional contribution of the stimulated cortex. Although this technique assumes that cortical stimulation operates by disrupting cortical function, its underlying mechanism is largely unknown. Hypotheses include electrophysiological mechanisms (disruption of synaptic activity, Nathan et al., 1993), neurochemical mechanisms (neurotransmitter depletion, Haycock et al., 1987), and neurovascular mechanisms (transient focal ischemia with a prolonged increase of Hbr, Suh et al., 2005).

Stimulation was performed for purely clinical purposes without any reference to possible scientific interpretation. Consequently, there was no systematic control for the possible confounding effects of site and stimulation parameters. Shown here are representative effects of stimulation between a cortical site adjacent to the laminar optodes, one proximal to the laminar optode recording with a longer stimulation period and one distal with a shorter stimulation period, to demonstrate the potential of this technique to measure changes in cortical processing and hemodynamics during different stimulation patterns.

The effects of short (500 ms) and long (5000 ms) duration stimulation trains on neural activity and hemodynamics are shown in Fig. 6. Single trial hemodynamics and CSD from both types of

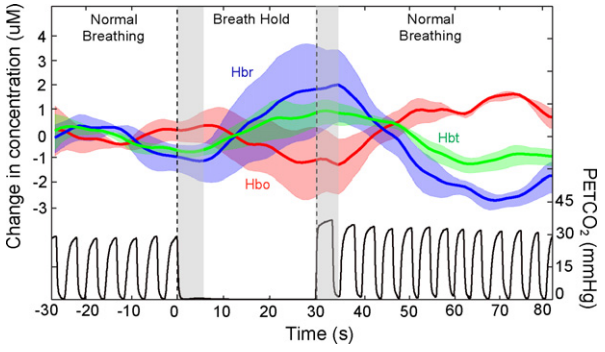

Fig. 5. Cerebral hemodynamics and PET_{CO_2} measured during a breath-hold challenge in one patient. Each of three cycles consisted of 30 s of breath-holding followed by 120 s of normal breathing. The plot shows the average hemodynamics and PET_{CO_2} values 30 s prior to until 80 s after stimulus onset. Hemodynamic parameters are measured in μM and PET_{CO_2} in mmHg. The colored transparent areas indicate one standard deviation above and below the averaged colored plot. Dotted lines represent the onset and termination of the breath-hold and the grey area after the dotted lines show the time latency before physiological change. Hbr and Hbt increased 5 s following onset of event, peaked 5 s after event, and gradually returned to baseline values. PET_{CO_2} values remained at 0 mmHg for the breath-hold duration and increased following breath-hold, confirming that the event was sufficiently long to elevate vascular CO_2 levels.

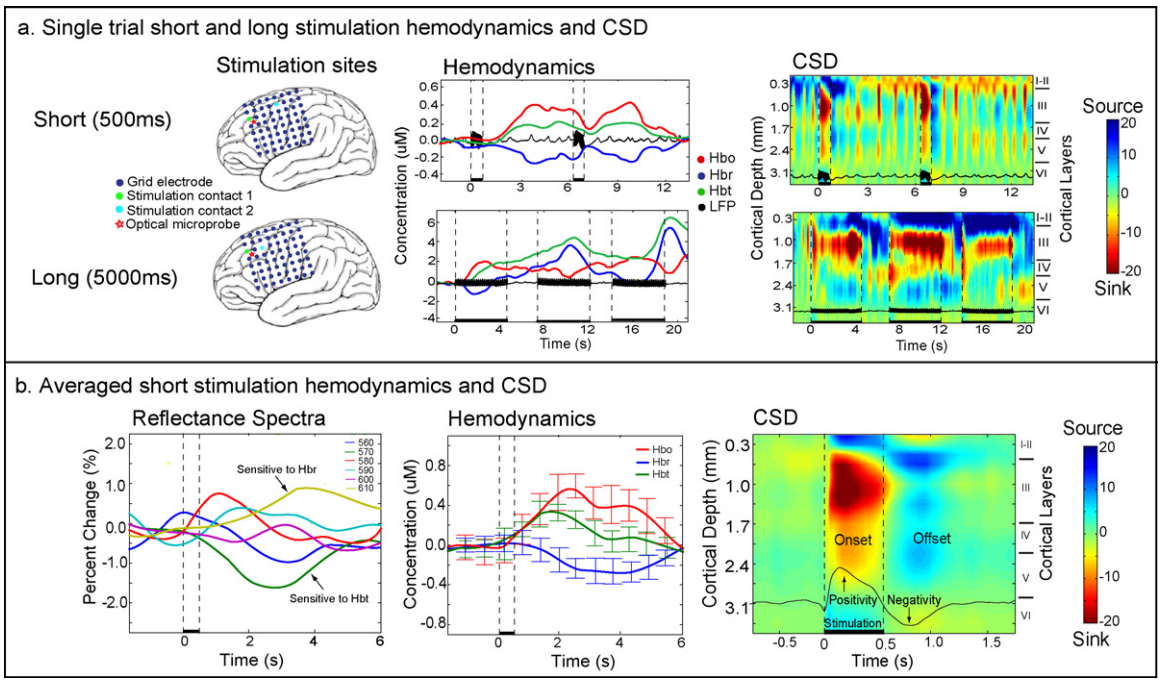

Fig. 6. Neural activity and hemodynamic changes recorded during cortical stimulation for functional mapping, in response to short (500 ms) and long (5000 ms) 50 Hz pulse trains. Pulses were symmetric and biphasic with 0.3 ms per phase. Pulses were applied between the contact immediately anterior to the laminar optode, and another grid location either ~4 cm or ~2 cm posterior for the short and long stimulation trains, respectively. Current source density (CSD) measures the trans-membrane current and identifies current sources (blue) and sinks (red) in cortical layers (scale is in *z*-score). Black dotted lines and bars represent the stimulus duration. (a) Single trial hemodynamics and CSD. Template brain maps indicate reference and stimulated intracranial grid electrodes and optical microprobe locations. Single trial hemodynamic changes demonstrate that while a short stimulus induces the expected increased oxygenation (presumably secondary to increased blood flow as suggested by increased total hemoglobin), longer stimulation causes increased deoxy-hemoglobin, with each stimulation accentuating the response. Single trial CSD plots show clear onset and offset response for short and long stimulus, while the long stimulus train is not as stereotyped. (b) Averaged reflectance spectra, hemodynamics, and CSD plots with the overlaid filtered local field potential of the superficial-most electrode. Following stimulation, reflectance increases at 610 nm and decreases at 570 nm, corresponding to an increase in Hbo and Hbt and a decrease in Hbr. Averaged CSD shows mirrored onset and offset source/sink pairs with a superficial positivity during the onset and negativity during the offset response. Multi-unit activity was recorded in this patient; however, due to the artifact during the stimulation phase, interpretation both during and directly following the stimulation was difficult and is not reported. A low-pass 30 Hz temporal filter minimized stimulus artifact in the CSD plots, and dotted black lines and black bars both denote the stimulation duration. Color CSD plots are observed in *z*-scores and error bars denote one standard deviation above and below the average. (For interpretation of the references to color in this figure legend, the reader is referred to the web version of the article.)

stimulation (Fig. 6a) as well as averaged reflectance spectra, hemodynamics, and CSD plots with overlaid local field potentials from the most superficial microelectrode contact from short stimulations (Fig. 6b) are shown. Multi-unit activity was recorded in this patient; however, due to the artifact during the stimulation phase, interpretation both during and directly following the stimulation was difficult and is not reported.

For the short stimulation, single trial hemodynamics show a local hyperoxidation peaking 3–4 s following stimulation with Hbo increasing ~0.4 μM, Hbr decreasing ~0.2 μM, and Hbt increasing ~0.2 μM (Fig. 6a). The corresponding CSD plot shows a stereotyped activity to the short stimulation with current sink/source pairs (sources in layers I–II, VI; sinks in III–V) during the stimulation (Fig. 6a). Averaged reflectance spectra, hemodynamics, and CSD plots for short stimulations are shown in Fig. 6b. The reflectance spectra used to calculate the associated hemodynamics show an increase in reflectance at 610 nm (sensitive to Hbr) and a decrease at 570 nm (sensitive to Hbt) following stimulation. Averaged hemodynamics demonstrate this local hyperoxidation following stimulation. Averaged CSD plots show a superficial positivity with current sink/source pairs (sources in I–II, VI; sinks in III–V) during the stimulation onset response and mirrored surface negativity with sink/source pairs (sources in III–V; sinks in I–II, VI) during the offset response (Fig. 6b).

Single trial hemodynamics to long stimulation trains shows strong contrasts to those of the short stimulation (Fig. 6a). Although, as would be expected, the initial hemodynamic responses to short or long trains are similar when they are preceded by a rest period, as the stimulation continues the initially decreased Hbr returns to zero and increases above baseline, indicating that the increased Hbt is no longer able to decrease Hbr concentration, and indeed is unable to keep pace with metabolic demand by this criterion. When a second long train follows shortly after the first, Hbr increases more, and an even larger increase is present to a third train in short succession. Hbt increases progressively, so Hbo never falls below baseline. The long stimulation condition causes hemodynamic changes that are 10 fold higher in amplitude than short stimulus pulses. These results further corroborate the hypothesis set forth by Suh et al. (2005) where increased stimulation amplitude results in increased Hbr. However, this response is not likely to be accompanied by ischemia as the concentration of oxygenated hemoglobin remains high.

The corresponding CSD plot shows similar sink/source pairs as in the shorter stimulation (sources in I–II, VI; sinks in III–V). However, following the initial onset response, the surface source deepens, the middle layered sink decreases in amplitude, and a new smaller amplitude current sink/source pair appears (source in IV–V, sink in VI) and continues for the duration of each stimulation. The offset response to the first stimulation in the train shows current sink/source pairs (sources in III, V; sinks in I–II, IV) which contrast the short stimulation offset response (Fig. 6b). Hemodynamic responses to long stimulations could not be averaged across stimulation trains, because they may take 40 s to return to baseline (see above), and clinical considerations dictated shorter delays between stimulus trains.

4. Discussion

4.1. Summary

Electrophysiological activities and cerebrovascular control processes are both extremely complicated. Despite the extensive use in clinical and research arenas, fMRI is not completely understood. fMRI is used mainly to study high level cognition in unanesthetized humans, while animals are preferred when studying low level sensory processes or anesthetized brains because electrophysiology may be measured directly. Thus, although the basic mechanisms of neurovascular coupling will need to be worked out in animal studies, studies in unanesthetized humans performing cognitive tasks will be important to validate these mechanisms and quantify their parameters in order to strongly interpret most fMRI experiments. The technique described here provides a means to measure the critical electrophysiological and hemodynamic variables simultaneously from the same small cortical volume, semi-chronically, with high spatial and temporal resolution in unanesthetized humans performing cognitive tasks.

The electrophysiological methodology (Ulbert et al., 2001a,b) has been validated in previously published experiments in humans during cognitive tasks (Ulbert et al., 2001a,b; Knake et al., 2007; Wang et al., 2005) and epilepsy (Ulbert et al., 2004). The validation efforts presented here thus concentrate on the spectroscopic and Doppler measures using evoking circumstances whose effects on hemodynamics are relatively well understood.

4.1.1. Electrocardiogram and cerebral blood flow

We have validated our laser Doppler flowmetry technique by observing its relationship to the heartbeat as measured by the simultaneously recorded EKG. As predicted, the heartbeat strongly modulated the rCBF inferred from laser Doppler, with the main rCBF peak occurring 150 ms following the *R*-peak in the QRS wave of the EKG, consistent with prior estimates of the vascular delay from the heart to the brain (Montgomery et al., 1995; Basano et al., 2001; Kucewicz et al., 2007). While latency time periods have been relatively consistent across studies, the direction and absolute size of the peak change from baseline is highly variable due to a number of reasons including measurement modality and location. Our device is placed in cortical grey matter relatively distant from arteries and veins, so measurements reported are most likely rCBF changes in capillaries, venules, and arterioles coursing nearby. As a result, it is unlikely that local recording of rCBF changes in microvasculature in humans have been reported and the 12% observed increase may in fact be a new finding.

4.1.2. Breath-holding

Breath-holding increases arterial CO_2, which in turn is known to produce vasodilation. The increased Hbt shown using point spectroscopy with the current technique is consistent with this vasodilation. In addition, the current data shows that this vasodilation is not sufficient to prevent a decrease in Hbo. The magnitude and direction of change during the breath-hold is relatively consistent with previous studies where an increase in both Hbr and Hbt on the order of a few μM has been observed (MacIntosh et al., 2003; Safonova et al., 2003). Although the direction of the hemodynamic change is consistent, the latency between event onset and the physiological change is less so. Wise et al. (2007) report a 5 s delay while MacIntosh et al. (2003) report a 20 s delay before hemodynamic changes. Kastrup et al. (1999) demonstrated that this discrepancy in latency can be explained by whether breath-holding is preceded by inspiration versus expiration. The dynamic changes reported here have an initial latency (∼5 s) between both the onset and termination of breath-holding to physiological changes, consistent with previous studies in humans (Safonova et al., 2003; Wise et al., 2007). Because we did not explicitly tell patients to inspire or expire directly before the hypercapnic event, this could account for the large variation between trials in this time period.

4.1.3. Cortical electrical stimulation

We recorded from the laminar optode during clinical cortical mapping using electrical stimulation of subdural electrodes. To our knowledge, these are the first measurements of neural processing and hemodynamics at the level of the cortical microcolumn during functional mapping at the patient's bedside. Preliminary results show differing neural and hemodynamic responses to short and longer stimulation. Both stimuli exhibit large initial current sink/source pairs, and the short stimuli exhibit an offset response that mirrors the stimulation onset. Unfortunately, multi-unit recordings were not available to inform interpretation of these current source/sink patterns as excitatory or inhibitory. However, comparison with unpublished laminar MUA and CSD recordings collected during controlled single-pulse electrical stimulation indicates that this layer III source in the offset response of the averaged short stimuli corresponds to neuronal inhibition consisting of outward (hyperpolarizing) current, decreased neuronal firing, and decreased high gamma power (Entz et al., 2007). Based on this preliminary data, the superficial positivity and presumably active current sink in middle cortical layers during the stimulation phase may describe cortical excitation and contribute to the increase in hyperoxygenation observed. In addition, the superficial negativity and passive current source observed during the offset response may describe cortical inhibition and have an inhibitory effect on the hemodynamic response.

An increase in Hbo and decrease in Hbr was observed peaking 3–4 s following the short stimulation train, while an increase in Hbr was observed following the long stimulation train. Although these stimulations also differed in the separation of the active stimulation electrode contacts, we hypothesize the differences between short and long stimulation trains result from the increased metabolic demand induced by the sustained stimulation. The hemodynamic changes could underlie some of the apparent cortical deficits induced by intense clinical stimulation (cf. Suh et al., 2005). However, due to the clinical nature of the functional mapping, the stimulation amplitude, duration, SOA, and contact spacing were confounded, and so these conclusions remain to be verified in a more controlled setting.

4.2. Potential applications

Semi-chronically implanting this device into the human neocortex for up to ten days has both basic science and clinical implications. Unlike intraoperative recordings of intrinsic signals or non-invasive imaging such as PET/fMRI, data can be collected in a relatively natural setting by the bedside of the patient. A variety of cortical states can be monitored including spontaneous recordings to study cortical oscillations, sleep studies, epileptiform discharges, functional motor and language mapping, as well as a variety of visual, auditory, and somatosensory tasks. Analyzing the neurovascular response from each of these recordings will enable us to obtain quantitative results of coupling in each of these cortical areas and disease states, essential as this relationship is not necessarily constant across modalities. Once this model is established, identical cognitive tasks and spontaneous recordings will be performed with fMRI and MEG, and a transfer function between this relationship at the local level recorded with the laminar optode and the global level can be determined. This model will allow non-invasive imaging conclusions to be made about cortical processing at the level of the microcolumn and not inferred as it is currently. In addition, we hope to shed light on the controversial topics of BOLD correlation to synaptic or spiking activity, stimulus-evoked negative

BOLD response, and the elusive "initial dip." We believe that this device can answer many of these fundamental questions that will strengthen fMRI interpretations.

The clinical significance and utility of this type of device is also substantial. Besides creating a model for interpreting non-invasive results such as pre-operative fMRI motor and language mapping, MEG source localization, and PET/SPECT used to localize regions indicative of epileptic cortex, we can develop a better understanding of functional mapping. Cortical stimulation involves many of the contacts on a subdural electrode grid, and by detecting the electrophysiological and neurovascular changes with the microprobe we can record measurements from different locations in the cortex. Therefore, when the patient undergoes motor and language mapping, we can develop a spatiotemporal model of electrophysiological, hemodynamic, and behavioral responses in order to further explore the mechanisms involved in the response to cortical stimulation.

In addition, this device may provide an essential insight into the controversy surrounding the onset and termination of seizures. It is generally accepted that epileptic seizures are associated with an increase in cerebral blood flow due to the abnormal firing rate of neurons (Penfield and Jasper, 1954). Studies have shown that generalized tonic-clonic seizures are associated with an approximate 20% increase in rCBF following seizure onset and a return to baseline levels after the seizure is resolved (Blumenfeld et al., 2003; Nersesyan et al., 2004). Nersesyan et al. (2004) further reports that spike-wave discharges in rats elicit an increase in focal neuronal activity and blood flow, while generalized tonic-clonic seizures are associated with more widespread blood flow increases. Recently, Zhao et al. (2007) were able to capture spontaneous electrographic seizures intraoperatively in the human motor cortex. They report an increase in Hbr and rCBF nearly 20 s preceding seizure onset. In addition, they found that blood flow was not sufficient to meet metabolic demand during the seizure. This device has recorded hemodynamics and electrophysiological signals during several ictal events to gain insight into the mechanisms involved in the onset, evolution, and termination of seizures.

4.3. Limitations

Although this device allows semi-chronic recording of intracortical electrophysiology and hemodynamics in a relatively natural setting with high spatial and temporal resolution, there are also several limitations of these recordings. First, the sampling area is limited to cortical columns proximal to the device. This problem could be partially resolved by placing multiple (up to four) devices into the cortex in order to sample from multiple cortical areas simultaneously. Second, accurate labeling of the cortical layers as well as evaluation of cortical pathology requires histology from the resected tissue. However, histology requires not only en bloc resection of the tissue surrounding the laminar optode, but also cooperation from medical staff which may not always be available. Lacking histology, the cortical layers can only be approximated and CSD interpretation is difficult. While histology was not performed in these patients, in other patients in which a similar device was implanted, histological examination showed relatively well-preserved tissue suggesting that the electrode pushes aside a column of tissue equal to its cross-section, thus minimizing the damage it imposes (Ulbert et al., 2001a,b). The total fluence of the optical components is well within safety standards for humans, and thus they are not likely to cause any additional damage (see Section 2.5). Finally, the microprobe is only placed in locations that are likely to be removed in the definitive surgery, and this would not include locations where removal would produce blindness, plegia, or aphasia. Consequently, it is unlikely that measurements with this device will be obtained in primary motor, sensory, or language cortices. However, the device can probe neurovascular coupling during important cognitive functions performed by association cortices lying outside of these highly eloquent areas.

5. Conclusions

We have developed a device that records detailed electrophysiological parameters in each cortical layer as well as blood flow and oxygenation of cortical microdomains in the unanaesthetized human cortex. EKG with simultaneous blood flow measurements and a breath-holding challenge confirm the validity of the recording techniques. In addition, preliminary results from electrophysiology and hemodynamic responses from cortical stimulation suggest differing responses from short and long stimulation. This device can provide insight into neurovascular coupling during cognitive tasks as well as clinical events such as functional mapping, sleep disorders, and seizures. In the near future we will be able to develop a quantitative model to interpret non-invasive results and apply this model to clinical events to gain a better understanding and lead to more effective treatments and therapies.

Acknowledgements

We would like to thank Andrew Dykstra, Alex Chan, Justine Cormier, and Nima Dehghani for excellent critique of this manuscript and László Papp for excellent technical support. This research is funded by NIH grants RO1-NS44623 and NS18741.

References

Attwell D, Iadecola C. The neural basis of functional brain imaging signals. Trends Neurosci 2002;25:621–5.
Basano L, Ottonello P, Nobili F, Vitali P, Pallavicini FB, Ricca B, et al. Pulsatile electrical impedance response from cerebrally dead adult patients is not a reliable tool for detecting cerebral perfusion changes. Physiol Meas 2001;22:341–9.
Blumenfeld H, Westerveld M, Ostroff RB, Vanderhill SD, Freeman J, Necochea A, et al. Selective fronal, parietal, and temporal networks in generalized seizures. Neuroimage 2003;19:1556–66.
Boas DA, Culver JP, Stott JJ, Dunn AK. Three Dimensional Monte Carlo code for Photon migration through complex heterogeneous media including the adult human head. Opt Express 2002;10:159–64.
Buxton R. The elusive initial dip. Neuroimage 2001;13:953–8.
Buxton RB, Wong EC, Frank LR. Dynamics of blood flow and oxygenation changes during brain activation: the balloon model. Magn Reson Med 1998;39:855–64.
Buzsaki G, Kaila K, Raichle M. Inhibition and brain work. Neuron 2007;56:771–83.
Bonner R, Nossal R. Model for laser Doppler measurements of blood flow in tissue. Appl Opt 1981;20:2097–107.
Custo A, Wells WM, Barnett AH, Hillman EMC, Boas DA. Effective scattering coefficient of the cerebral spinal fluid in adult head models for diffuse optical imaging. Appl Opt 2006;45:4747–55.
Devor A, Dunn AK, Andermann ML, Ulbert I, Boas DA, Dale AM. Coupling of total hemoglobin concentration, oxygenation, and neural activity in rat somatosensory cortex. Neuron 2003;39:353–9.
Devor A, Tian P, Nishimura N, Teng IC, Hillman EM, Narayanan SN, et al. Suppressed neuronal activity and concurrent arteriolar vasoconstriction may explain negative blood oxygenation level-dependent signal. J Neurosci 2007;27:4452–9.
Dunn AK, Devor A, Dale AM, Boas DA. Spatial extent of oxygen metabolism and hemodynamic changes during functional activation of the rat somatosensory cortex. Neuroimage 2005;27:279–90.
Einevoll GT, Pettersen KH, Devor A, Ulbert I, Halgren E, Dale AM. Laminar population analysis: estimating firing rates and evoked synaptic activity from multielectrode recordings in rat barrel cortex. J Neurophysiol 2007;97:2174–90.
Entz L, Fabo D, Eross L, Halasz P, Wittner L, Karmos G, Halgren E, Ulbert I. Inhibitory effects of cortical electrical stimulation in epileptic patients. Society for Neuroscience, Nov 2007.
Felleman DJ, VanEssen DC. Distributed hierarchical processing in the primate cerebral cortex. Cereb Cortex 1991;1:1–47.
Freeman JA, Nicholson C. Experimental optimization of current source-density technique for anuran cerebellum. J Neurophysiol 1975;38:369–82.
Grubb Jr RL, Raichle ME, Eichling JO, Ter-Pogossian MM. The effects of changes in $PaCO_2$ on cerebral blood volume, blood flow, and vascular mean transit time. Stroke 1974;5:630–9.
Haglund MM, Hochman DW. Optical imaging of epileptiform activity in human neocortex. Epilepsia 2004;45:43–7.
Halgren E, Walter RD, Cherlow DG. Mental phenomena evoked by electrical stimulation of the human hippocampal formation and amygdale. Brain 1978a;101:83–117.

Halgren E, Wilson CL, Stapleton JM. Human medial temporal-lobe stimulation disrupts both formation and retrieval of recent memories. Brain Cogn 1978b;4: 287–95.
Haycock JW, Levy WB, Cotman CW. Stimulation dependent depression of neurotransmitter release in the brain:[Ca] dependence. Brain Res 1987;155:192–5.
Heeger DJ, Huk AC, Geisler WS, Albrecht DG. Spikes versus BOLD: what does neuroimaging tell us about neuronal activity? Nat Neurosci 2000;3:631–3.
Holsheimer J. Electrical conductivity of the hippocampal CA1 layers and application to current-source-density analysis. Exp Brain Res 1987;67:402–10.
Jones M, Berwick J, Johnston D, Mayhew J. Concurrent optical imaging spectroscopy and laser-Doppler flowmetry: the relationship between blood flow, oxygenation, and volume in rodent barrel cortex. NeuroImage 2001;13:1002–15.
Jones M, Hewson-Stoate N, Martindale J, Redgrave P, Mayhew J. Nonlinear coupling of neural activity and CBF in rodent barrel cortex. NeuroImage 2004;22: 956–65.
Kastrup A, Ti T, Glover GH, Moseley ME. Cerebral blood flow-related signal changes during breath-holding. Am J Neuroradiol 1999;20:1233–8.
Knake S, Wang CM, Ulbert I, Schomer DL, Halgren E. Specific increase of human entorhinal population synaptic and neuronal activity during retrieval. Neuroimage 2007;37:618–22.
Kohl M, Lindauer U, Royl G, Kuhl M, Gold L, Villringer A, et al. Physical model for the spectroscopic analysis of cortical intrinsic optical signals. Phys Med Biol 2000;45:3749–64.
Kucewicz JC, Dunmire B, Leotta DF, Panagiotides H, Paun M, Beach KW. Functional tissue pulsatility imaging of the brain during visual stimulation. Ultrasound Med Biol 2007;33:681–90.
Lesser RP, Luders H, Klem G, Dinner DS, Morris HH, Hahn JF, et al. Extraoperative cortical functional localization in patients with epilepsy. J Clin Neurophysiol 1987;4:27–53.
Lindauer U, Royl G, Leithner C, Kuhl M, Gethmann GL, Kohl-Bareis M, et al. No evidence for early decrease in blood oxygenation in rat whisker cortex in response to functional activation. Neuroimage 2001;13:986–99.
Logothesis NK, Pauls J, Augath M, Trinath T, Oeltermann A. Neurophysiological investigation of the basis of the fMRI signal. Nature 2001;412:150–7.
Logothesis NK, Wandell BA. Interpreting the BOLD signal. Ann Rev Physiol 2004;66:735–69.
Logothesis NK. The ins and outs of fMRI signals. Nat Neurosci 2007;10:1230–2.
Logothesis NK. The underpinning of the BOLD functional magnetic resonance imaging signal. J Neurosci 2003;23:3963–71.
MacIntosh BJ, Klassen LM, Menon RS. Transient hemodynamics during a breath hold challenge in a two part functional imaging study with simultaneous near-infrared spectroscopy in adult humans. NeuroImage 2003;20:1246–52.
Mandeville JB, Marota JJ, Ayata C, Moskowitz MA, Weisskoff RM, Rosen BR. MRI measurement of the temporal evolution of relative CMRO(2) during rat forepaw stimulation. Magn Reson Med 1999;42:944–51.
Martindale J, Mayhew J, Berwick J, Jones M, Martin C, Johnston D, et al. The hemodynamic impulse response to a single neural event. J Cereb Blood Flow Metab 2003;23:546–55.
Mayhew J, Johnston D, Berwick J, Jones M, Coffey P, Zheng Y. Spectroscopic analysis of neural activity in brain: increased oxygen consumption following activation of barrel cortex. Neuroimage 2000;12:664–75.
Mitzdorf U. Current source-density method and application in cat cerebral cortex: investigation of evoked potentials and EEG phenomena. Physiol Rev 1985;65:37–100.
Montgomery LD, Montgomery RW, Guisado R. Rheoencephalographic and electroencepthalographic measures of cognitive workload: analytical procedures. Biol Phychol 1995;40:143–59.
Mukamel R, Gelbard H, Arieli A, Hasson U, Fried I, Malach R. Coupling between neuronal firing, field potentials, and FMRI in human auditory cortex. Science 2005;309:951–4.
Murakami S, Zhang T, Hirose A, Okada YC. Physiological origins of evoked magnetic fields and extracellular field potentials produced by guinea-pig CA3 hippocampal slices. J Physiol 2002;544:237–51.
Nair DG. About being BOLD. Brain Res Rev 2005;50:229–43.
Nathan SS, Sinha SR, Gordon B, Lesser RP, Thakor NV. Determination of current density generated by electrical stimulation of the human cerebral cortex. Electroencephalogr Clin Neurophysiol 1993;86(3):193–292.
Nicholson C, Freeman JA. Theory of current source-density analysis and determination of conductivity tensor for anuran cerebellum. J Neurophysiol 1975;38: 356–68.
Nersesyan H, Herman P, Erdogan E, Hyder F, Blumenfeld H. Relative changes in cerebral blood flow and neuronal activity in local microdomains during generalized seizures. J Cereb Blood Flow Metab 2004;24:1057–68.
Ogawa S, Lee TM, Kay AR, Tank DW. Brain magnetic resonance imaging with contrast dependent on blood oxygenation. Proc Natl Acad Sci USA 1990;87:9868–72.
Ojemann GA. Cortical organization of language. J Neurosci 1991;11:2281–7.
Patterson MS, Andersson-Engels S, Wilson BC, Osei EK. Absorption spectroscopy in tissue-simulating materials: a theoretical and experimental study of photon paths. Appl Opt 1995;34:22–30.
Peterson KH, Devor A, Ulbert I, Dale AM, Einevoll GT. Current-source density estimation based on inversion of electrostatic forward solution: Effects of finite extent of neuronal activity and conductivity discontinuities. J Neurosci Methods 2006;154:116–23.
Rees G, Friston K, Koch C. A direct quantitative relationship between the functional properties of human and macaque V5. Nat Neurosci 2000;3:716–23.
Sassaroli A, Martelli F, Fantini S. Perurbation theory for the diffusion equation by use of the moments of the generalized temporal point spread function. II. Continuous wave results. JOSA A 2006;23:2119–31.
Safonova LP, Michalos A, Wolf U, Choi JH, Wolf M, Mantulin WW, et al. Diminished cerebral circulatory autoregulation in obstructive sleep apnea investigated by near-infrared spectroscopy. Sleep Res Online 2003;5:123–32.
Schmuel A, Augath M, Oeltermann A, Logothesis NK. Negative functional MRI response correlates with decreases in neuronal activity in monkey visual area V1. Nat Neurosci 2006;9:569–77.
Schroeder CE, Mehta AD, Givre SJ. A spatiotemporal profile of visual system activation revealed by current source density analysis in the awake macaque. Cereb Cortex 1998;8:575–92.
Suh M, Bahar S, Mehta AD, Schwartz TH. Temporal dependence in uncoupling of blood volume and oxygenation during interictal epileptiform events in rat neocortex. J Neurosci 2005;25:68–77.
Thomason ME, Burrows BE, Gabrieli JDE, Glover GH. Breath holding reveals differences in fMRI BOLD signal in children and adults. NeuroImage 2005;25:824–37.
Ulbert I, Karmos G, Heit G, Halgren E. Early discrimination of coherent versus incoherent motion by multiunit and synaptic activity in human putative MT+. Hum Brain Mapp 2001a;13:226–38.
Ulbert I, Halgren E, Heit G, Karmos G. Multiple microelectrode-recording system for human intracortical applications. J Neurosci Methods 2001b;106:69–79.
Ulbert I, Heit G, Madsen J, Karmos G, Halgren E. Laminar analysis of human neocortical interictal spike generation and propagation: current source density and multiunit analysis in vivo. Epilepsia 2004;45:48–56.
Vanzetta I, Grinvald A. Increased cortical oxidative metabolism due to sensory stimulation: implications for functional brain imaging. Science 1999;286:1555–8.
Waldvogel D, van Gelderen P, Muellbacher W, Ziemann U, Immisch I, Hallett M. The relative metabolic demand of inhibition and excitation. Nature 2000;406:995–8.
Wang C, Ulbert I, Ives JR, Schomer DL, Blume H, Marinkovic K, et al. Responses of human anterior cingulated cortex microdomains to error detection, conflict monitoring, stimulus-response mapping, familiarity, and orienting. J Neurosci 2005;25:604–13.
Wise RG, Pattinson KTS, Bulte DP, Chiarelli PA, Mayhew SD, Balanos GM, et al. Dynamic forcing of end-tidal carbon dioxide and oxygen applied to functional magnetic resonance imaging. J Cereb Blood Flow Metab 2007;27:1521–32.
Wray S, Cope M, Delpy DT, Wyatt JS, Reynolds EO. Characterization of the near infrared absorption spectra of cytochrome aa3 and haemoglobin for the non-invasive monitoring of cerebral oxygenation. Biochim Biophys Acta 1988;933:184092.
Xie A, Skatrud JB, Khayat R, Dempsey JA, Morgan B, Russell D. Cerebrovascular response to carbon dioxide in patients with congestive heart failure. Am J Resp Crit Care Med 2005;172:371–8.
Zhang R, Levine BD. Autonomic ganglionic blockade does not prevent reduction in cerebral blood flow velocity during orthostasis in humans. Stroke 2006;38:1238–44.
Zhao M, Suh M, Ma M, Perry C, Geneslaw A, Schwartz TH. Decreases in focal perfusion and hemoglobin oxygenation precede seizure onset in spontaneous human lesional epilepsy. Epilepsia 2007;48:2059–67.